SUPPRESING NOISE IN QUANTUM COMPUTING OF ELECTRONIC STRUCTURE OF CRYSTALS

Jan HOJAČ[1,2], Vojtěch VAŠINA[1,3], Martin FRIÁK[1,2]

[1]*Institute of Physics of Materials, v. v. i., Czech Academy of Sciences, Žižkova 22, Brno, 616 00, Czech Republic, EU, hojac@ipm.cz, vasina@ipm.cz, friak@ipm.cz;*

[2]*Department of Condensed Matter Physics, Faculty of Science, Masaryk University, Brno, Czech Republic, EU*

[3]*Institute of Material Science and Engineering, Faculty of Mechanical Engineering, Brno University of Technology, Brno, Czech Republic, EU*

https://doi.org/10.37904/nanocon.2025.5189

Abstract

Quantum computing is currently emerging as a new computational technology for solving complex computational problems. Current quantum computers are unfortunately too noisy to provide sufficient accuracy, and quantum-classical hybrid algorithms emerged as a solution. Variational Quantum Algorithms are currently showing promising results at overcoming noise introduced by the current level of quantum hardware. Variational Quantum Deflation (VQD) has gained significant attention when computing the full spectrum of eigenvalues in quantum chemistry and solid-state physics. The noise in the VQD calculations performed on the current noisy quantum computers, or their simulators, can be partly suppressed by methods available in the Qiskit Python package provided by IBM. In our study, several error suppression and mitigation methods have been tested, and our results offer a unique comparison in the case of calculations on the electronic structure of crystals, where performance is sensitive to the actual point in the reciprocal space.

Keywords: Quantum computing, variational quantum deflation, noise, electronic band structure

1. INTRODUCTION

The electronic band structure of a crystal is a central subject in solid-state physics, as it determines many of the material's fundamental properties. Accurate calculations of electronic energy levels are therefore essential in a wide range of applications. For simple systems, sufficiently precise band structures can be obtained with exact Hamiltonian diagonalization on classical computers. However, as the system size increases, the computational cost grows rapidly, making such calculations increasingly demanding.

Quantum computers offer a potential way forward. Thanks to their inherently quantum nature, qubits provide a more natural framework for simulating electronic systems. At present, though, quantum computations remain prone to various types of noise. To mitigate this limitation, hybrid classical-quantum algorithms have been developed, combining the strengths of both approaches.

In this work, we calculate the electronic band structure of a gallium arsenide (GaAs) crystal using the Variational Quantum Deflation (VQD) algorithm [1]. We explore two representations of the system: first, encoding the Hamiltonian as a ten-qubit quantum circuit, and second, reducing it to a four-qubit model. Both cases were simulated under realistic quantum hardware noise. Noise model used in the calculations has been imported from the quantum processing unit *ibm_brisbane* from IBM Quantum Platform [2]. Particular attention is given to the relationship between absolute error and computation time under different conditions.

2. SYSTEM DESCRIPTION

To determine the band structure of GaAs, it is necessary to obtain a Hamiltonian of the system. One of the most frequent tools is the so-called tight-binding method, whose description might be found in Ashcroft [3]. The tight-binding Hamiltonian of gallium arsenide will not be calculated explicitly here, instead we will use one from [4], given by the following matrix:

$$\hat{H} = \begin{bmatrix} E_{s,a} & V_{s,s}g_0 & 0 & 0 & 0 & V_{sa,pc}g_1 & V_{sa,pc}g_2 & V_{sa,pc}g_3 & 0 & 0 \\ V_{s,s}g_0^* & E_{s,c} & -V_{sa,pc}g_1^* & -V_{sa,pc}g_2^* & -V_{sa,pc}g_3^* & 0 & 0 & 0 & 0 & 0 \\ 0 & -V_{sa,pc}g_1 & E_{p,a} & 0 & 0 & V_{x,x}g_0 & V_{x,y}g_3 & V_{x,y}g_2 & 0 & -V_{pa,s^*c}g_1 \\ 0 & -V_{sa,pc}g_2 & 0 & E_{p,a} & 0 & V_{x,y}g_3 & V_{x,x}g_0 & V_{x,y}g_1 & 0 & -V_{pa,s^*c}g_2 \\ 0 & -V_{sa,pc}g_3 & 0 & 0 & E_{p,a} & V_{x,y}g_2 & V_{x,y}g_1 & V_{x,x}g_0 & 0 & -V_{pa,s^*c}g_3 \\ V_{sa,pc}g_1^* & 0 & V_{x,x}g_0^* & V_{x,y}g_3^* & V_{x,y}g_2^* & E_{p,c} & 0 & 0 & V_{s^*a,pc}g_1 & 0 \\ V_{sa,pc}g_2^* & 0 & V_{x,y}g_3^* & V_{x,x}g_0^* & V_{x,y}g_1^* & 0 & E_{p,c} & 0 & V_{s^*a,pc}g_2 & 0 \\ V_{sa,pc}g_3^* & 0 & V_{x,y}g_2^* & V_{x,y}g_1^* & V_{x,x}g_0^* & 0 & 0 & E_{p,c} & V_{s^*a,pc}g_3 & 0 \\ 0 & 0 & 0 & 0 & 0 & V_{s^*a,pc}g_1^* & V_{s^*a,pc}g_2^* & V_{s^*a,pc}g_3^* & E_{s^*,a} & V_{s^*,s^*}g_0 \\ 0 & 0 & -V_{pa,s^*c}g_1^* & -V_{pa,s^*c}g_2^* & -V_{pa,s^*c}g_3^* & 0 & 0 & 0 & V_{s^*,s^*}g_0^* & E_{s^*,a} \end{bmatrix}$$

(1)

The constants appearing in the Hamiltonian can be looked up in [4] and they have the following values:

$$\begin{aligned} E_{\mathrm{s,a}} &= -8.34\ \mathrm{eV}, & E_{\mathrm{p,a}} &= +1.04\ \mathrm{eV}, \\ E_{\mathrm{s,c}} &= -2.66\ \mathrm{eV}, & E_{\mathrm{p,c}} &= +3.67\ \mathrm{eV}, \\ E_{\mathrm{s^*,a}} &= +8.59\ \mathrm{eV}, & E_{\mathrm{s^*,c}} &= +6.74\ \mathrm{eV}, \\ V_{\mathrm{s,s}} &= -6.45\ \mathrm{eV}, & V_{x,x} &= +1.95\ \mathrm{eV}, \\ V_{x,y} &= +5.08\ \mathrm{eV}, & V_{\mathrm{sa,pc}} &= +4.48\ \mathrm{eV}, \\ V_{\mathrm{sc,pa}} &= +5.78\ \mathrm{eV}, & V_{\mathrm{s^*a,pc}} &= +4.84\ \mathrm{eV}, \\ V_{\mathrm{pa,s^*c}} &= +4.81\ \mathrm{eV}, & a_{\mathrm{L}} &= +5.65\ \text{Å}. \end{aligned}$$

While the lattice parameter a_L is not explicitly seen in the matrix, it is important to correctly determine the phase contributions g_0, g_1, g_2, g_3, which are given by

$$\begin{aligned} 4g_0(\vec{k}) &= e^{i\vec{k}\cdot\overrightarrow{d_0}} + e^{i\vec{k}\cdot\overrightarrow{d_1}} + e^{i\vec{k}\cdot\overrightarrow{d_2}} + e^{i\vec{k}\cdot\overrightarrow{d_3}}, \\ 4g_1(\vec{k}) &= e^{i\vec{k}\cdot\overrightarrow{d_0}} + e^{i\vec{k}\cdot\overrightarrow{d_1}} - e^{i\vec{k}\cdot\overrightarrow{d_2}} - e^{i\vec{k}\cdot\overrightarrow{d_3}}, \\ 4g_2(\vec{k}) &= e^{i\vec{k}\cdot\overrightarrow{d_0}} - e^{i\vec{k}\cdot\overrightarrow{d_1}} + e^{i\vec{k}\cdot\overrightarrow{d_2}} - e^{i\vec{k}\cdot\overrightarrow{d_3}}, \\ 4g_3(\vec{k}) &= e^{i\vec{k}\cdot\overrightarrow{d_0}} - e^{i\vec{k}\cdot\overrightarrow{d_1}} - e^{i\vec{k}\cdot\overrightarrow{d_2}} + e^{i\vec{k}\cdot\overrightarrow{d_3}}. \end{aligned} \quad (2)$$

The vector $\vec{k}$ is an arbitrary wavevector from the first Brillouin zone and the vectors $\overrightarrow{d_0}$, $\overrightarrow{d_1}$, $\overrightarrow{d_2}$, $\overrightarrow{d_3}$ are the positions of atoms which are nearest to the one located at the origin (i.e. its nearest neighbours). As gallium arsenide crystallizes in the zinc blende structure, those positions are $\overrightarrow{d_0} = \left(\frac{a_L}{4}, \frac{a_L}{4}, \frac{a_L}{4}\right)$, $\overrightarrow{d_1} = \left(\frac{a_L}{4}, -\frac{a_L}{4}, -\frac{a_L}{4}\right)$, $\overrightarrow{d_2} = \left(-\frac{a_L}{4}, \frac{a_L}{4}, -\frac{a_L}{4}\right)$, $\overrightarrow{d_3} = \left(-\frac{a_L}{4}, -\frac{a_L}{4}, \frac{a_L}{4}\right)$.

3. METHODS

We employ the VQD algorithm to obtain energy eigenvalues. Let us introduce a set of *n* variational parameters $\vec{\theta} = (\vartheta_1, \vartheta_2, \cdots, \vartheta_n)$, such that the trial states of the Hamiltonian depend explicitly on these parameters. In accordance with the variational principle (see, e.g., Zettili [5]), the ground state is determined by minimizing the functional $\langle\psi(\vec{\theta})|\hat{H}|\psi(\vec{\theta})\rangle$. The *m*-th excited state is then obtained by minimizing the cost function

$$C_m(\vec{\theta}) = \langle\psi(\vec{\theta})|\hat{H}|\psi(\vec{\theta})\rangle + \sum_{j=0}^{m-1}\beta_j|\langle\psi(\vec{\theta})|\psi_j\rangle|^2, \quad (3)$$

where the penalty coefficients β_j suppress overlaps with the previously determined eigenstates $\{\psi_j\}$.

Although the penalty parameters β_j do not have unique prescribed values, they should be chosen sufficiently large – at least on the order of the spacing between consecutive energy levels – to ensure that the optimization avoids convergence to already identified states. For a more detailed description of the algorithm, we refer the reader to [6].

3.1. Ten-qubit approach

One way to translate Hamiltonian (1) into a quantum circuit is by using a ten-qubit register. At first glance, this may appear counterintuitive, since it amounts to embedding a 10 x 10 Hamiltonian into a 1024 x 1024 space. However, with a suitable ansatz a 1014-dimensional subspace remains inert, and the Hamiltonian acts non-trivially only on the subspace spanned by the ten computational basis states of interest.

A convenient choice for this purpose is a diagonal ansatz (**Figure 1**; discussion of different ansatzes may be found in [7]), which has been well described in, for example, in Ref. [8].

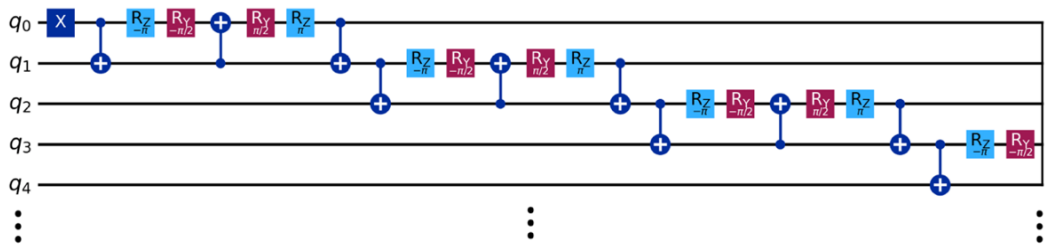

Figure 1 Visualization of the diagonal ansatz with 1-qubit gates X, R_z, R_y and 2-qubit entangling gates.

3.2. Four-qubit approach

An alternative approach uses the fact that a 16-dimensional Hamiltonian can be represented exactly with four qubits as $2^4 = 16$. For Hamiltonians whose dimension is not a power of two, we embed them as

$$\hat{H}' = \hat{H} \oplus h\widehat{I_H}, \tag{4}$$

where h = 20 eV, exceeds the largest eigenvalue. Here, $\widehat{I_H}$ is an identity matrix of dimension

$$\dim(\widehat{I_H}) = \exp\left(\left\lceil \log_2(\dim(\hat{H}))\right\rceil \ln 2\right) - \dim(\hat{H}), \tag{5}$$

so that $\hat{H}'$ has the smallest power-of-two dimension not less than $\hat{H}$.

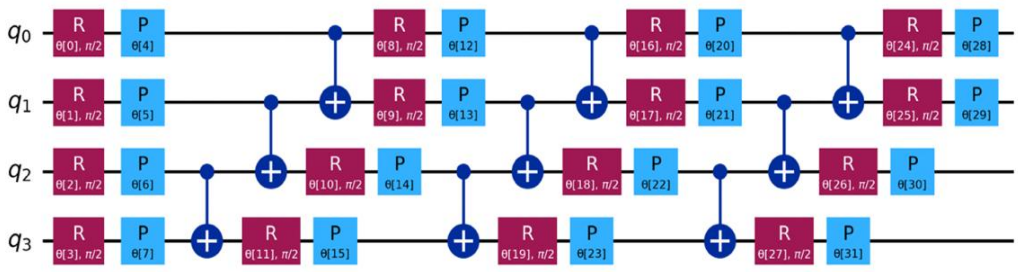

Figure 2 Visualization of the EfficientSU2 ansatz.

This embedding enables the representation with the minimal number of qubits, while the added high-energy band remains isolated and does not affect the system directly. The EfficientSU2 ansatz [9] is used for the implementation on four qubits, as shown in **Figure 2**.

4. RESULTS

Figures below present the calculated band structures (BS) of GaAs obtained using the previously described ansatzes. **Figure 3** and **Figure 5** show results from the four-qubit implementation, while **Figure 4** and **Figure 6** correspond to the ten-qubit case. All these simulations were performed without noise. In contrast, **Figure 7** and **Figure 8** display the four-qubit BS including a noise model derived from the *ibm_brisbane* quantum processor [2], where a pronounced loss of accuracy is evident even after many iterations. In all cases, a roughly linear increase in computation time with higher band indices is observed, likely due to the growing number of overlap evaluations required by the VQD algorithm.

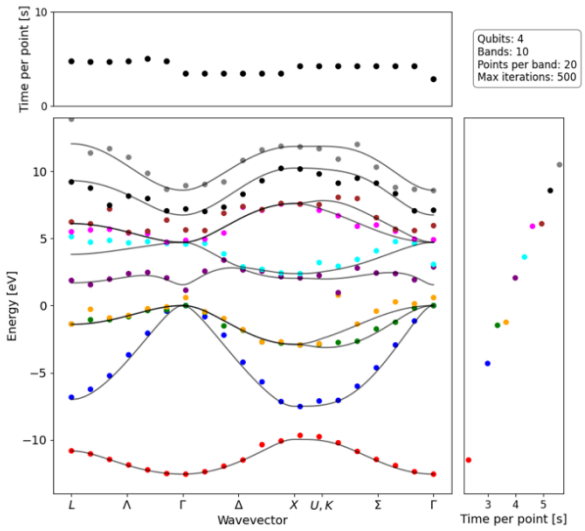

Figure 3 4-qubit BS, 500 iterations

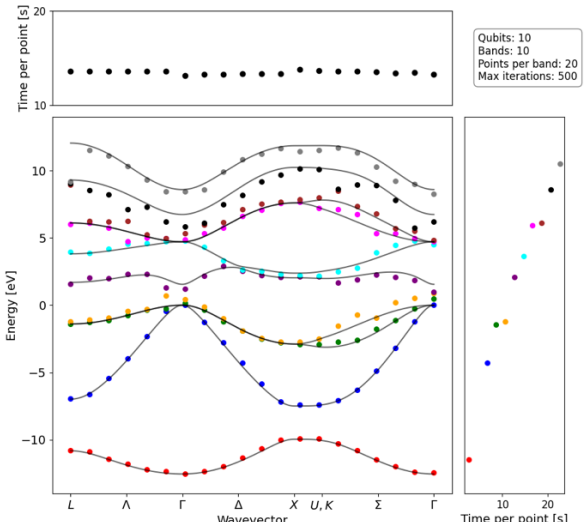

Figure 4 10-qubit BS, 500 iterations

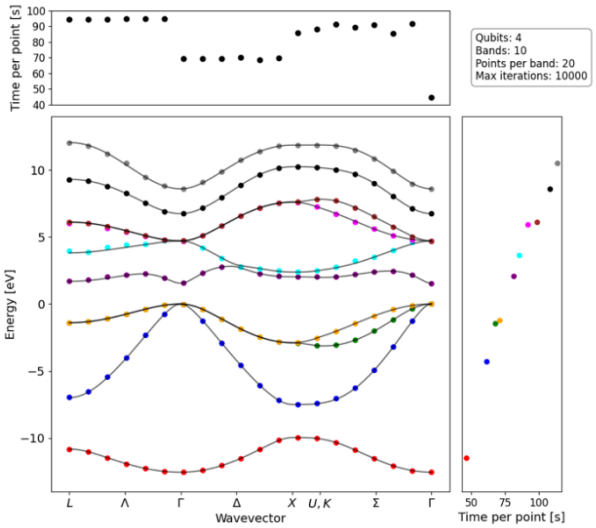

Figure 5 4-qubit BS, 10000 iterations

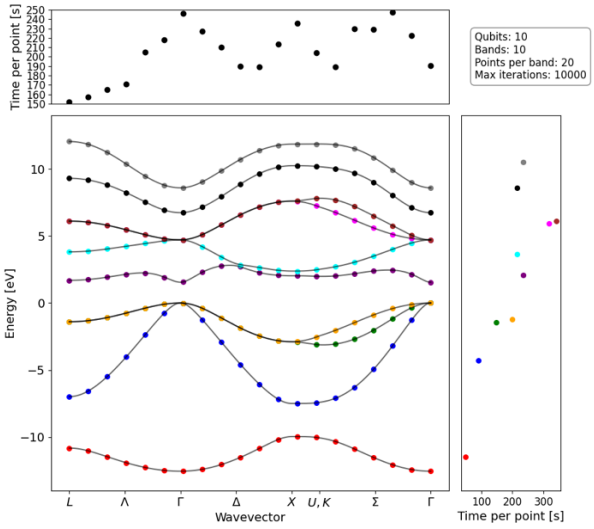

Figure 6 10-qubit BS, 10000 iterations

Figure 9 illustrates a clear power-law dependence between computation time and error for bands 1, 2 and 10 in the noiseless regime; however, this trend is obscured by noise as shown in **Figure 10**. Our analysis demonstrates that realistic hardware noise acts as the dominant limiting factor, disrupting the power-law convergence in the reduced 4-qubit model. This indicates that reproducing the chemical accuracy achieved

via hyperparameter optimization in the noiseless study of Ref. [8] is unattainable on current hardware without robust error mitigation.

CONCLUSION

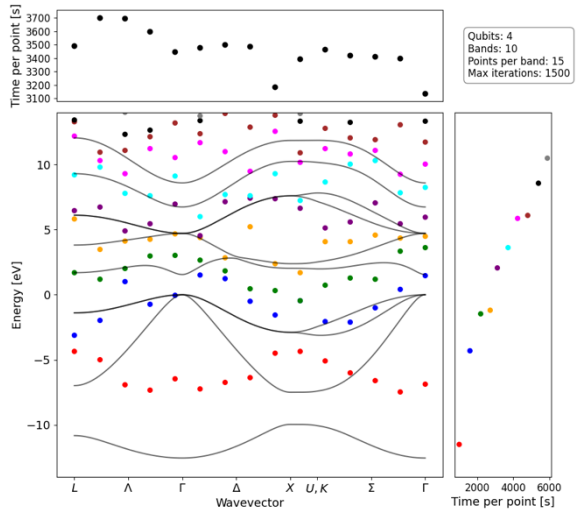

Figure 7 4-qubit BS, 1500 iterations, noise

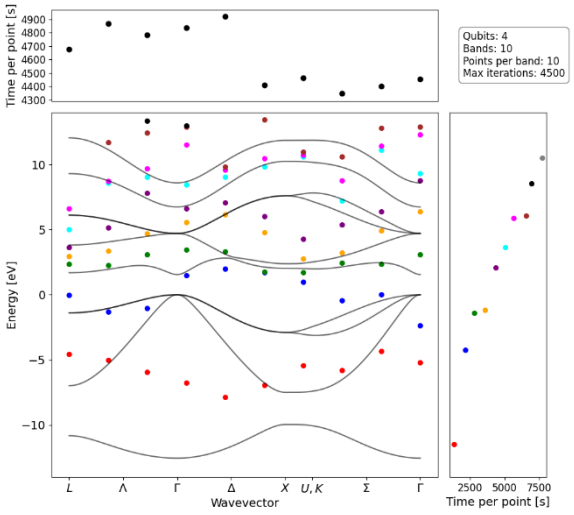

Figure 8 4-qubit BS, 4500 iterations, noise

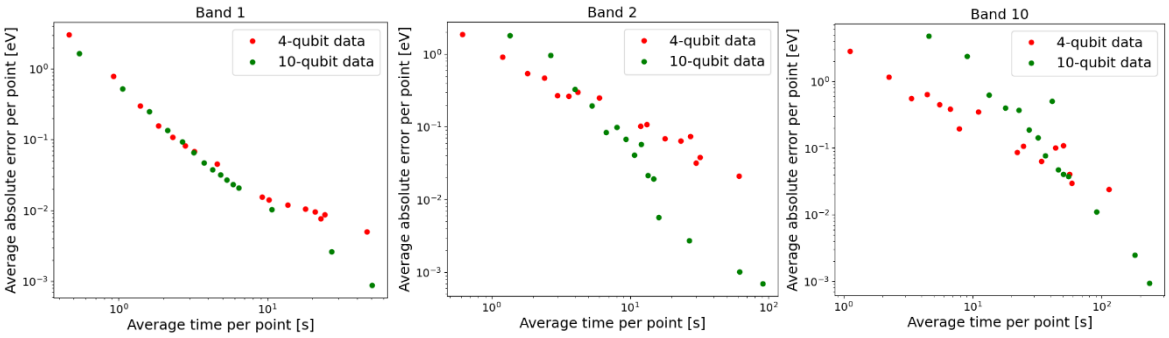

Figure 9 Average time needed to a given absolute error in given bands. Logarithmic scale, no noise

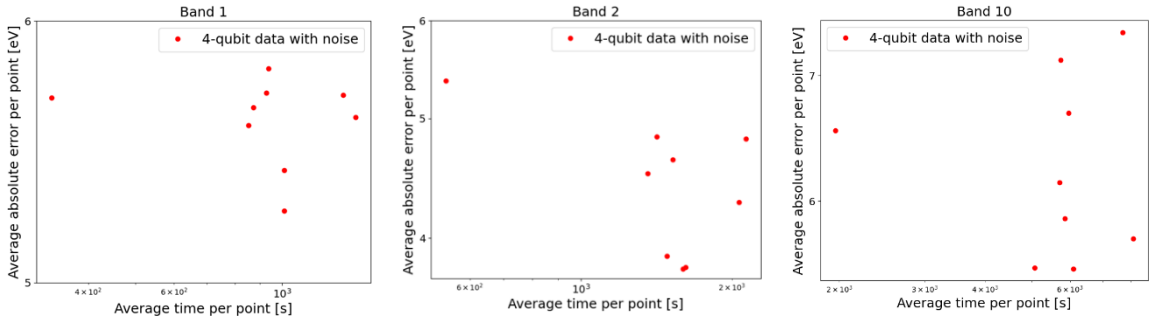

Figure 10 Average time needed to a given absolute error in given bands. Logarithmic scale, noise included

In this study, we examined the feasibility of computing electronic band structures using the VQD algorithm. A 10x10 Hamiltonian was mapped onto both four- and ten-qubit quantum circuits. The four-qubit case was simulated with and without noise, while the ten-qubit system was considered only in the noiseless regime. The noiseless simulations demonstrate that quantum algorithms can accurately reproduce classical band

structures, with both implementations yielding consistent results. As shown in **Figure 9**, mapping a 10-dimensional Hamiltonian directly to a 10-qubit circuit provides a time advantage when high accuracy is required. Conversely, logarithmic reduction to four qubits offers faster computation when approximate results suffice. When noise is included, the simulations capture the general trends but lose quantitative agreement with reference data. This is evident in **Figure 7** and **Figure 8**, where even thousands of iterations fail to ensure good VQD convergence. **Figure 10** further highlights this effect, showing that the power-law behaviour observed in the noiseless case (**Figure 9**) is largely suppressed by noise. Our work demonstrates both the potential and current limitations of quantum computing for electronic band-structure simulations. VQD-based results capture key physical features in noiseless conditions but degrade under realistic noise. Ongoing advances in quantum hardware and error mitigation are expected to make such simulations increasingly more practical for systems beyond classical scalability.

ACKNOWLEDGEMENTS

Financial supports from the Czech Academy of Science are gratefully acknowledged, in particular the Praemium Academiae awarded to MF and the Strategy AV21 (the program "AI: Artificial Intelligence for Science and Society"). The authors further acknowledge financial supports from (i) The Ministry of Education, Youth and Sports via the INTER-EXCELLENCE II program, sub-program INTER-COST, in particular the project No. LUC25028, and (ii) the Quantum Innovative Centre providing us the access to the IBM quantum computers. Computational resources were provided by the Ministry of Education, Youth and Sports of the Czech Republic under the Projects e-INFRA CZ (ID:90254) at the IT4Innovations National Supercomputing Center and e-Infrastruktura CZ (e-INFRA LM2018140) at the MetaCentrum as well as CERIT Scientific Cloud, all provided within the program Projects of Large Research, Development and Innovations Infrastructures.

REFERENCES

[1] HIGGOT, O., WANG, D., BRIERLEY, S. Variational Quantum Computation of Excited States. *Quantum.* 2019, vol. 3, pp. 156 – 166.

[2] IBM Quantum. *Compute resources.* [online]. 2025 [viewed: 2025-10-10]. Available from: https://quantum.cloud.ibm.com/computers?order=backend_name.

[3] ASHCROFT, N.W., MERMIN, N.D., *Solid State Physics*. Philadelphia: Saunders College, 1976.

[4] VOGL, P., HJALMARSON, H.P., DOW, J.D. A Semi-empirical tight-binding theory of the electronic structure of semiconductors. *Journal of Physics and Chemistry of Solids*. 1983, vol. 44, no. 5, pp- 365-378. Available from: https://doi.org/10.1016/0022-3697(83)90064-1.

[5] ZETTILI, N. Quantum Mechanics: *Concepts and Applications*. Chichester: Wiley, 2009.

[6] IBM Quantum. *Instances and extensions*. [online]. 2025 [viewed: 2025-09-10]. Available from: https://quantum.cloud.ibm.com/learning/en/courses/variational-algorithm-design/instances-and-extensions.

[7] IBM Quantum. *Ansaetze and variational forms*. [online]. 2025 [viewed: 2025-09-10]. Available from: https://quantum.cloud.ibm.com/learning/en/courses/variational-algorithm-design/ansaetze-and-variational-forms.

[8] MIHÁLIKOVÁ, I., KREJČÍ, M., FRIÁK, M. The impact of quantum circuit architecture and hyperparameters on variational quantum algorithms exemplified in the electronic structure of the GaAs crystal. *Scientific reports*. 2025, 15, 15746. https://doi.org/10.1038/s41598-025-00151-x.

[9] IBM Quantum Documentation. *EfficientSU2.* [online]. 2025 [viewed: 2025-09-10]. Available from: https://quantum.cloud.ibm.com/docs/en/api/qiskit/qiskit.circuit.library.EfficientSU2.